Journal Name

RSCPublishing

ARTICLE

Bio-inspired carbon nitride mesoporous spheres for artificial photosynthesis: photocatalytic cofactor regeneration for sustainable enzymatic synthesis

Cite this: DOI: 10.1039/x0xx00000x

Received 00th January 2012, Accepted 00th January 2012

DOI: 10.1039/x0xx00000x

www.rsc.org/

Jianhui Huang,[b] Markus Antonietti[a] and Jian Liu[a]*

Inspired by photosynthetic thylakoid membrane of chloroplasts, we present here the rational design of mesoporous structured colloids made up of graphitic carbon nitride nanosheet and demonstrate their application in photocatalytic NADH regeneration for sustainable enzymatic synthesis.

Introduction

High efficiency light energy-to-chemicals conversion is thought to be the ultimate goal in the field of sustainable energy, considering the sustainable and inexhaustible character of sunlight.[1] In natural photosynthesis, green plants and algae have evolved highly delicate, complex structures to convert light to chemical energy. Learning from nature might offer some possible key elements for realizing artificial photosynthesis.[2-6] Inside the photosynthetic factories termed chloroplasts, a membrane-bound thylakoid is the site of the light-dependent reactions of photosynthesis. Following light harvesting by chlorophyll molecules, photoinduced electrons are passed through electron transport chain to the enzyme ferredoxin-NADP (nicotinamide adenine dinucleotide phosphate) reductase, leading to the reduction of NAD(P) to NAD(P)H, completing the storage of light energy in one kind of "energy currency" of the cells (another kind is ATP). The newly formed NAD(P)H is used as hydrogen source with high reducing power for the biosynthesis of carbohydrates from CO_2 in the Calvin cycle of the dark reaction.[7] $NAD(P)^+$/NAD(P)H cofactors are also involved in many other enzymatic redox reactions of the metabolism. Recently, applying such enzymatic redox reactions for the synthesis of valuable and chiral compounds in vitro became highly attractive.[8-10] However, high costs of enzyme-specific cofactors (NADH) hinder wider applications, and sustainable and economically acceptable regeneration methods for NADH are still eagerly demanded.[11]

As in the photosynthetic light reactions, using light energy for the reduction of NAD^+ to NADH is very promising and inherently sustainable, comparing with the established but not optimal enzymatic regeneration method and electrochemical routes.[12-16] Taking electrons from light excited photocatalyst and coupling the proton to form the hydride electron pair, the NAD^+ can be selectively reduced to 1,4-NADH in the presence of $[Cp^*Rh(bpy)H_2O]^{2+}$ (abbreviated as **M** in the following context) acting as hydride transfer reagent while triethanolamine (denoted as TEOA) is employed as sacrificial electron donor.[17] Despite of previously reported works on the photocatalytic NADH regeneration, however, more facile and more efficient visible-light-driven photocatalytic system are critically needed and are to be developed.[18-23]

Inspired by the folded, layered thylakoid membranes featuring very large surface area, which therefore could increase the amount of light absorbance, construction of a structural mimicry of the thylakoid membranes as a semiconductor object is promising to increase the efficiency of NADH regeneration.[24] Graphitic carbon nitride (abbreviated as $g\text{-}C_3N_4$) is known as a layered material and found in recent years to possess visible-light-driven photocatalytic properties.[25-32] Our previous work demonstrated that a synthetic carbon nitride photosynthetic structure onto diatom frustules could be used for photocatalytic NADH regeneration.[33] However, the low surface area partly counterbalanced the benefits of refractive light harvesting brought by the diatom structure.[34] Higher efficiency could be achieved by coupling a higher specific surface area and strong light harvesting properties.[35] Carbon nitride will act as the ultimate light-to-charge pair conversion site while a structured mesoporous sphere architecture could enhance the light intensity onto the active centers.[36-38] The in-situ regenerated NADH is then coupled with L-lactate dehydrogenase for sustainable photoenzymatic synthesis. In addition, as outlined in our previous report, direct transfer of hydride electron pair from carbon nitride to NAD^+ is also possible, and metal- and mediator free regeneration of NADH as the ultimate goal will also be investigated.[39]

Experimental section

Materials synthesis

Synthesis of CNMS: In a typical synthesis, 5 mL TEOS was injected into a mixture of 20 mL of deionized H_2O, 5 mL of $NH_3 \bullet H_2O$ and 100 mL 2-propanol at room temperature under magnetic stirring. After reacting for 2 hours, the colloidal spheres were collected by centrifugation, re-dispersed in 150 mL deionized water. Certain amount of polyvinylpyrrolidone (PVP) K15 (Mw ~ 10,000) was added to the above SiO_2 solution. The mixture was heated up to 100°C and kept for 3 hours under refluxing to load PVP, and then cooled to room temperature. Under magnetic stirring, 37.5 mL of 0.1 g/mL sodium hydroxide aqueous solution was added to the as-cooled solution at room temperature. As more material is etched away from the silica particles, the solution becomes less and less opaque. The etching process could be monitored by measuring transmission of the etching solution at 700 nm using UV-Vis spectrometry. A mixture of 1 g of etched SiO_2 mesoporous sphere and 5 g of cyanamide was degassed for 3 hours followed by sonication in water for 2 hours. After remove surplus cyanamide by water dissolving, the obtained white solid was transferred to a crucible with lid and heated under air at 2.3 °C min^{-1} up to 550 °C (4 hours) and kept at 550 °C for another 4 hours. The resultant yellow powder is treated with 4 M NH_4HF_2 solution for 48 hours. The dispersion is then filtered and the yellow precipitate is copiously rinsed with deionized water and ethanol. Finally, the yellow powder is dried under vacuum at 60 °C overnight.

Synthesis of $[Cp^*Rh(bpy)H_2O]^{2+}$: $RhCl_3 \cdot H_2O$ is refluxed in methanol with one equivalent of 1, 2, 3, 4, 5-Pentamethylcyclopentadiene for 24 hours. The resulting red precipitate is filtrated and suspended in methanol. On addition of two equivalents of 2, 2-bipyridine, the suspension clears up immediately and a yellowish solution is formed. $[Cp^*Rh(bpy)Cl]Cl$ is precipitated on the addition of diethyl ether into the obtained yellowish solution. Stock solutions (100 mM) are prepared in water and stored at room temperature avoiding direct light exposure. $[Cp^*Rh(bpy)Cl]Cl$ readily hydrolyzes to $[Cp^*Rh(bpy)(H_2O)]^{2+}$.

Characterization

XRD measurements were performed on a D8 Diffractometer from Bruker instruments (Cu Kα radiation, λ = 0.154 nm) equipped with a scintillation counter. N_2 sorption experiments were done with a Quantachrome Autosorb-1 at liquid nitrogen temperature. TEM images were taken on Philips CM200 FEG (Field Emission Gun), operated at an acceleration voltage of 200 kV. SEM measurement was performed on a LEO 1550 Gemini instrument. The UV-Vis absorbance spectra were recorded on a T70 UV/Vis spectrophotometer. The FTIR spectrum was collected using a Varian 1000 FTIR spectrometer.

Electrochemical analysis: The working electrode was prepared on indium-tin oxide (ITO) glasses, which was cleaned by sonication in chloroform, acetone and ethanol for 30 min, respectively. The glass was then rinsed with Millipore water and kept in isopropanol for 24 h. 50 mg powder was mixed with 2 mL dimethylformamide under sonication for 30 min to get slurry. The slurry was spreading onto ITO glass whose side part was previously protected using Scotch tape. After air drying, the electrode was fired at 350 °C for 30 min in air to improve adhesion. A copper wire was connected to the side part of the ITO glass using a conductive tape. Uncoated parts of the electrode were isolated with epoxy resin, and the exposed area of the electrode was 0.25 cm^2. Electrochemical measurements were performed in a conventional three electrode cell, using a Pt plate and a Ag/AgCl electrode (3 M KCl) as counter electrode and reference electrode, respectively. The electrolyte was a 0.2 M Na_2SO_4 aqueous solution without additive and was purged with nitrogen gas for 2 h prior to the measurements. The working electrodes were immersed in the electrolyte for 60 s before any measurement was taken. The photocurrent measurements were conducted with a BAS Epsilon workstation, with the working electrodes irradiated from the back side in order to minimize the influence of thickness of the semiconductor layer. The light was generated by a 500w xenon lamp (Changtuo, CHF-XM500) with a 420nm cut-off filter, and was chopped manually (≈0.20 Hz). The electrochemical impedance spectroscopy experiments were taken on a Precision PARC workstation. For Nyquist plots measurements, the perturbation signal were also 20 mV but the frequency ranged from 200 KHz to 10 mHz.

NADH regeneration and photoenzymatic reaction

NADH regeneration: In a typical regeneration procedure, the reaction medium was composed of NAD^+ (1 mM), TEOA (15 w/v%), phosphate buffer (100 mM) and carbon nitride materials. The pH value of the reaction media were set to 8 or 10 for mediator involved or mediator free system, respectively. The reaction system was placed into a quartz reactor equipped with stirring bar and illuminated with LED lamp (wavelength=420 nm, OSA Opto Light GmbH). The distance between reactor and LED lamp is fixed at 5 cm. Before the illumination, the reaction solution was placed in dark environment for certain minutes to achieve adsorption-desorption equilibrium. During the illumination, the concentration of NADH was calculated by measuring the absorbance of diluted reaction system at 340 nm. NAD^+ has peak absorption at a wavelength of 260 nm, with an extinction coefficient of 16,900 $M^{-1} \cdot cm^{-1}$. NADH has peak absorption at 340 nm with an extinction coefficient of 6,220 $M^{-1} \cdot cm^{-1}$.

Photoenzymatic reaction: The reaction medium for the photoenzymatic reaction includes NAD^+ (1 mM), M (0.25 mM), pyruvate (5 mM), L-Lactate dehydrogenase (50 U), pH=7.0 phosphate buffer with 15 w/v% TEOA, 3 mg CNMS. The reaction solution was stirred in the dark for one hour followed 6 hours light reaction.

Results and discussion

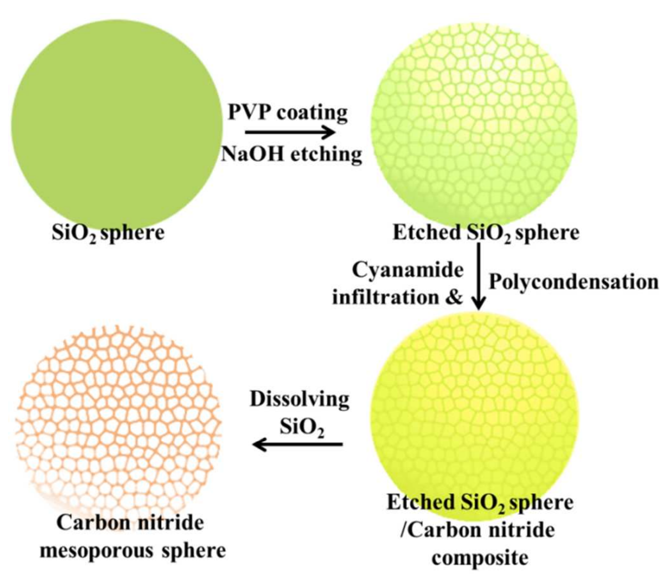

Scheme 1 Schematic fabrication strategy for CNMS. The whole processes could be divided into four steps: 1) Synthesis of SiO_2 sphere; 2) Loading with PVP under refluxing condition and mildly etch PVP coated SiO_2 with NaOH to obtain mesoporous SiO_2; 3) Loading cyanamide precursor into porous space followed by in-situ thermal condensation to carbon nitride; 4) Using NH_4HF_2 aqueous solution to release CNMS.

Carbon nitride mesoporous spheres (abbreviated as CNMS) were synthesized by templating etched silica spheres, adopting a strategy termed "silica-etching chemistry", as illustrated in **Scheme 1**.[40] Briefly, the SiO_2 sphere was firstly loaded with polyvinylpyrrolidone (PVP) for protecting an outside SiO_2 shell, and sodium hydroxide solution mildly etches the dense silica sphere towards a mesoporous system. This etched mesoporous structures then provides confined and necessary space for loading the cyanamide precursor for the subsequent in-situ thermal condensation towards carbon nitride. At last, after removing the silica template by aqueous NH_4HF_2 solution, a CNMS preserving the original sphere size, but with inverted inner structure could be obtained.[26] In general, the moderation and control of the silica-etching chemistry is the determining factor for the successful construction of CNMS. The degree of etching can be facilely controlled by the etching time; an appropriate etching end point can be quantitatively determined by an increase of the original optical transmission at 700 nm wavelength up to 70%. The morphology evolution of SiO_2 sphere during different etching times was investigated, as illustrated in **Figure S1** of Electronic Supplementary Information (ESI). Different etching degrees of SiO_2 lead to entirely different morphologies of the obtained carbon nitride materials. As templated from the original SiO_2 sphere or SiO_2 sphere with low etching degree, only fragments and no defined particles could be obtained.

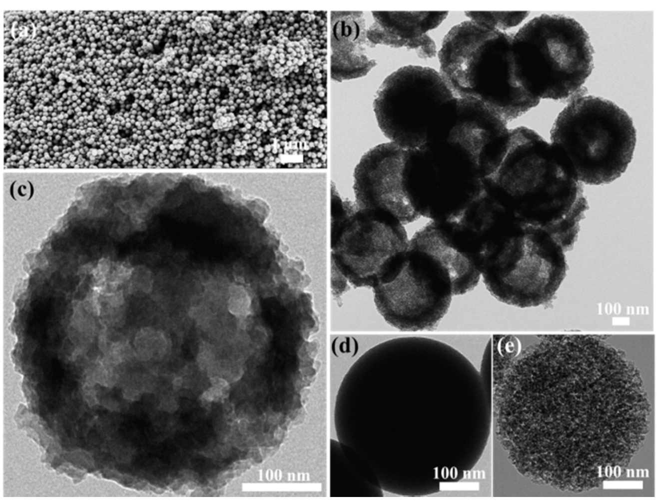

Figure 1. (a) SEM image of large area overview, illustrating the uniform and monodisperse properties of CNMS. (b) TEM image of CNMSs. (c) TEM image of a single CNMS particle, showing the porous property and nanosheet as the building blocks of CNMS. (d) and (e) show the TEM images of original solid SiO_2 sphere and etched mesoporous SiO_2 sphere, respectively.

Scanning electron microscopy (SEM) and Transmission Electron Microscopy (TEM) images in low magnification for a large area overview of CNMS demonstrate the high homogeneity and uniformity of obtained spherical material, as shown in **Figure 1a and 1b,** and the local structure was evidenced by TEM image shown in **Figure 1c**. The CNMS was chosen to have a diameter around 420 nm to enable multiple internal light reflections and consequently higher light absorbance. The size matches with the peak wavelength of the blue LED light source which also is near the onset of optical absorbance of $g\text{-}C_3N_4$. The original SiO_2 and etched SiO_2 spheres are compared to those replicated structures in **Figure 1d&e,** while the corresponding SEM images along with large overview of CNMS are displayed in **Figure S2** of ESI, respectively. Throughout etching, the PVP protected SiO_2 spheres do not decrease in diameter. The solid spheres turn to mesoporous with the coarsened surface while still preserving the spherical morphology, indicating the etching process is prohibited by the PVP protection of the shell. Compared with the sphere template, the size of obtained CNMS is a little smaller due to the shrinkage throughout thermal condensation. The typical material characterization results for CNMS are presented in **Figure S3** of ESI. The band at 810 cm^{-1} in the Fourier transform infrared spectroscopy (FTIR) spectra in **Figure S3a** of ESI is ascribed to the s-triazine ring modes, while the bands at 1200~1600 cm^{-1} are characteristics of aromatic CN heterocycles. Powder X-ray diffraction (XRD) spectrum shows the two characteristic peaks of graphitic carbon nitride (**Figure S3b** of ESI at 13.0º and 27.4º which are ascribed to the in-planar repeat period and stacking of the conjugated aromatic system, respectively. N_2 sorption measurement reveals the CNMS is indeed mesoporous, with a specific surface area of 205 m^2/g (see **Table 1**, **Figure S3** and **S4** of ESI).

Table 1. *Textural properties of $g\text{-}C_3N_4$ prepared under different conditions.*

sample	Bulk $g\text{-}C_3N_4$	$mpg\text{-}C_3N_4$	CNMS
Surface area[a] (m^2/g)	12	230	205
Pore volume[b] (cm^3g^{-1})	0.21	0.765	0.51
C/N ratio [c]	0.676	0.679	0.682
Hydrogen content[d] (%)	2.06	2.45	2.31

[a] BET surface area, [b] Barrett-Joyner-Halenda (BJH) adsorption pore volume, [c] Molar ratio, [d] Weight ratio.

The (photo)electrochemical properties of CNMS accompanying with two control samples (bulk $g\text{-}C_3N_4$ and $mpg\text{-}C_3N_4$) were investigated by electrochemical impedance spectroscopy (**Figure 2a**). The results revealed semicircular Nyquist plots for CNMS, $mpg\text{-}C_3N_4$ and $g\text{-}C_3N_4$ with the trend of increasing diameter, which demonstrated that CNMS possessed an improved electronic conductivity already in the dark state as compared to the other morphologies. The photoinduced electron transfer processes were also investigated. The photocurrent measurements of the three materials casted on indium tin oxide glass were conducted in 0.2 M Na_2SO_4 aqueous solution (**Figure 2b**). Large enhancement of I_{ph} for CNMS was indeed observed over an applied bias potential of 0.4 V versus Ag/AgCl, indicating strong light harvesting capability and faster transport of charged carriers.

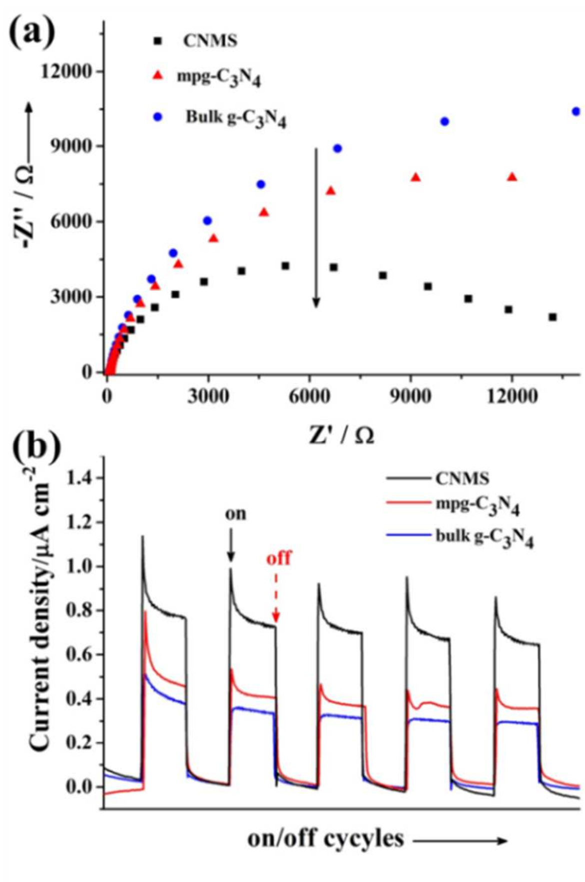

Figure 2. (a) Electrochemical impedance spectroscopy Nyquist plots for CNMS, mpg-C_3N_4 and g-C_3N_4, respectively. (b) The periodic on/off photocurrent output of CNMS, mpg-C_3N_4 and g-C_3N_4 casted on ITO glass at 0.4 V bias vs. Ag/AgCl in a 0.2 M Na_2SO_4 solution.

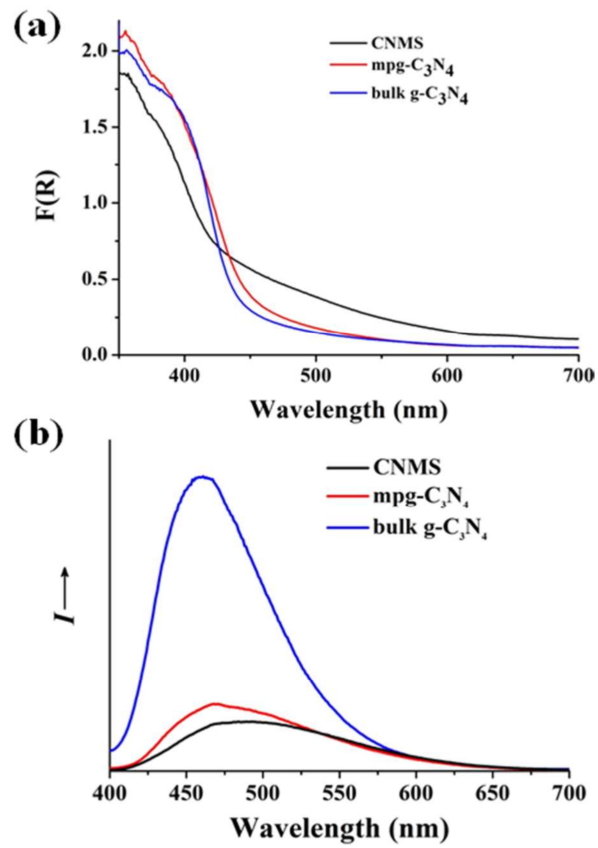

Figure 3. (a) Optical absorption of CNMS, mpg-C_3N_4 and g-C_3N_4 samples, respectively. (b) The photoluminescence spectra of CNMS, mpg-C_3N_4 and g-C_3N_4 samples.

Figure 3a shows the diffuse reflectance spectra of the obtained materials, indicating typical semiconductor absorption behavior. The slight blue shift of CNMS in the optical absorption relative to bulk g-C_3N_4 might be ascribed to the smaller structural size of the nanosheet building block (see **Figure 1c** and **Figure S5** of ESI). The CNMS also exhibited a stronger absorption than two reference samples, especially in the 420-500 nm wavelength regions. Photoluminescence spectrum, coming from the recombination of free charge carriers, usually serves as a good technique for evaluating the processes of charge migration, transfer and separation. As illustrated in **Figure 3b,** as compared to bulk g-C_3N_4, the substantially decreased fluorescence emission intensity of CNMS around 470 nm indicated the suppressed recombination rate of the photoinduced charge carriers, which is beneficial for further photocatalytic application.[26,41] The time-resolved photoluminescence spectrum was also employed to understand the photophysical behaviors of photoexcited charge carriers (**Figure S6** of ESI). The fluorescent intensities of all three samples decay exponentially. A lifetime of ~6 ns was obtained for CNMS at room temperature (298 K), which gives an estimate for the time for charges to reach the surface stabilized sites and the related structural length scales of a few nanometers.

Based on the above photo- and electrochemical investigations of CNMS, the photocatalytic NADH regeneration was performed. Optimum reaction conditions were adopted from our previous work.[33] A reaction solution with pH value at 8 in phosphate buffer solution with 15% TEOA was employed. **M** is a homogeneous redox catalyst acting as hydride transfer reagent to shuffle hydride to the NAD^+. An active carbon nitride content of 3 mg was maintained in all the experiments. The NADH regeneration was determined by measuring the increase of absorbance at 340 nm (with a molar extinction coefficient of 6,220 $M^{-1}\cdot cm^{-1}$) using Lambert-Beer law, as illustrated in **Figure S7** of ESI.

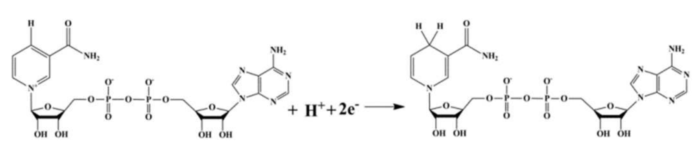

Scheme 2. The summarized reaction equation shows the regeneration of NADH.

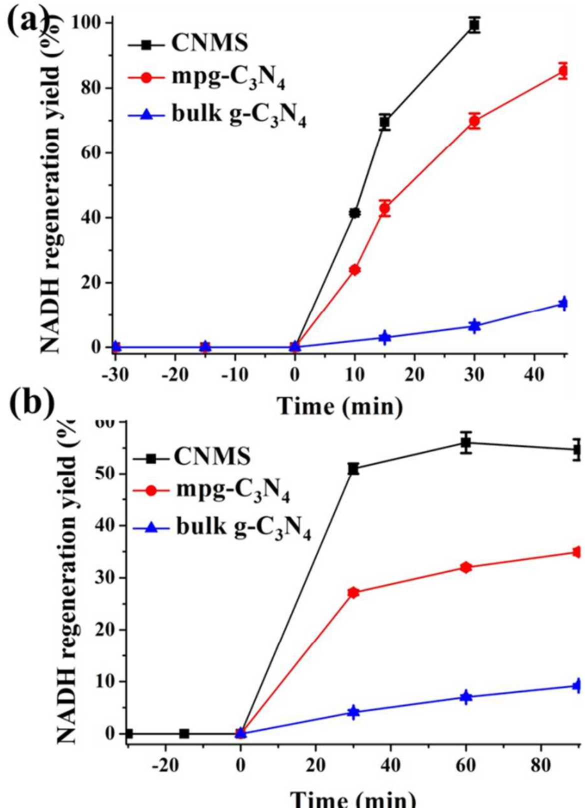

Figure 4. (a) Photocatalytic NADH regeneration kinetics in the presence of **M** (a) and Mediator free (b) by CNMS, mpg-C_3N_4 and g-C_3N_4, respectively. For (a), mediator involved NADH regeneration: β-NAD^+, 1 mM; M, 0.25 mM; TEOA, 15 w/v%; PBS buffer, 0.1 M, pH=8; carbon nitride, 3 mg; For (b), mediator free NADH regeneration: β-NAD^+, 1 mM; TEOA, 15 w/v%; PBS buffer, 0.1 M, pH=10; carbon nitride, 3 mg.

The regeneration of NADH from NAD^+ is summarized in the reaction equation in **Scheme 2**. The photocatalytic activity comparisons among CNMS, mpg-C_3N_4 and bulk g-C_3N_4 are presented in **Figure 4a**. During the first illumination period, the conversion yields increase linearly. Under the same circumstance, typical well-known semiconductors such as TiO_2 and ZnO were both inactive for NADH regeneration during the same illumination time. For comparison, no NADH regeneration took place in the dark. CNMS gives the best performance, and the NADH conversion yield reached to 100% after only 30 min light illumination. mpg-C_3N_4 and g-C_3N_4 give 80% and 10% conversion yield within the same illumination period, respectively. Considering the even smaller surface area of CNMS compared to mpg-C_3N_4 (see **Figure S4** and **Table 1**), the higher activity can be ascribed to structural features which improve the light harvesting by inner reflections and field enhancement effects.[42-44] High efficiency light harvesting by CNMS leads to more light-generated electron carriers, which are subsequently transferred to **M** to couple with proton, then shuffled to NAD^+ to create 1, 4-NADH.

Even more striking, under alkaline reaction conditions (pH=10) the CNMS regenerates NADH in 50% percent yield without an electron mediator under light after only 30 minutes (**Figure 4b**). This again demonstrates the excellent performance of CNMS as a photocatalytic system for NADH regeneration. The direct hydride transfer between CNMS and NAD^+ substrate is possibly promoted by the π-π stacking interaction between adenine subunit of β-NAD^+ and the electron-rich, layered configurations of g-C_3N_4, as the

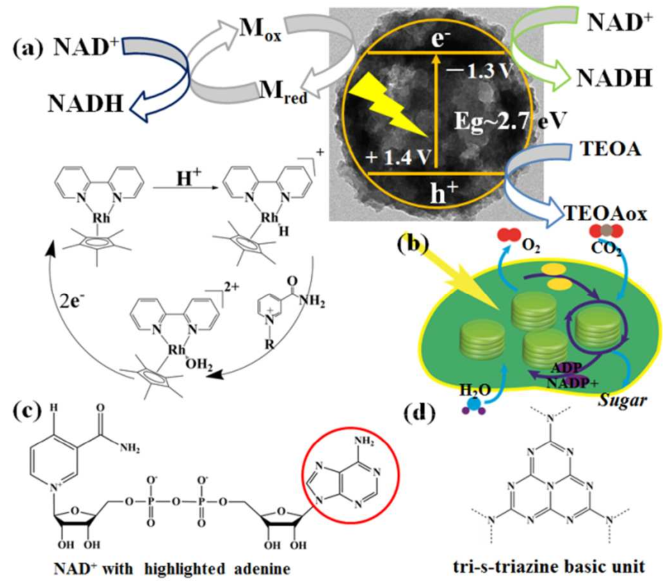

Figure 5. (a) Schematic illustration of photocatalytic NADH regeneration by CNMS, including mediator involved system and mediator free system, respectively. The regeneration of catalytically active $[Cp^*Rh(bpy)(H)]^+$was also illustrated, which acts as hydride transfer reagent towards NAD^+.(b) The thylakoid structure and NADPH involved functions in photosynthetic chloroplast under light irradiation.(c) The molecular structure of β-NAD^+ with adenine group highlighted in a red circle. (d) A perfect graphitic carbon nitride constructed from tri-s-triazine building blocks was illustrated.

building block of CNMS.[45-47] For the mpg-C_3N_4, a 50% percent conversion yield was only achieved after two hours illumination. After 30 min illumination, only 25% of conversion yield were reached. It is worth mentioning that regeneration for NADH in the mediator free system is accompanied by the loss of stereospecificity, and the 1, 6- and 1, 4-isomers are formed simultaneously.

The mechanism of photocatalytic NADH regeneration process and the photosynthetic light reactions are illustrated in **Figure 5a&b, respectively**. Under light excitation, CNMS generates electron/hole pairs. **M** can selectively regenerate 1, 4-NADH by taking two electrons from the CNMS (-1.3 V vs. NHE, pH=7) followed by coupling with one proton and regiospecific transfer to NAD^+ (-0.3 V vs. NHE) (See H NMR of **M** in **Figure S8** of ESI). More specifically, the electrons are transferred to $[Cp^*Rh(bpy)(H_2O)]^{2+}$, producing Cp*Rh(bpy), followed by coupling with one proton to form the hydriderhodium $[Cp^*Rh(bpy)(H)]^+$, which acts as hydride transfer reagent towards NAD^+. Due to the coordination of ring-slipped η^3-$[Cp^*Rh(bpy)(H)]^+$ at the carbonyl-C-atom of oxidized NAD^+, the enzymatically active 1, 4-NADH isomer is exclusively generated. The holes (+1.4 V vs. NHE) take their electrons from the oxidation of TEOA (-0.84 V vs. NHE), producing glycolaldehyde and di(ethanol)amine.[21] The g-C_3N_4 network featuring tri-s-triazine units as building blocks and the molecular structure of the NAD^+ with the highlighted adenine subunit are presented in **Figure 5c&d**, respectively. The π-π stacking interaction leads to the hydride transfer from g-C_3N_4 to NAD^+ and the subsequent NADH regeneration but with poor selectivity for enzymatically active 1, 4-isomer. Upon taking the electron from CNMS, NAD^+ could be reduced to NAD•, and the free radical might undergo proton-assisted disproportionation to form 1, 6-NADH. Only minor amounts of enzymatic active 1, 4-NADH can be obtained via the isomerization by non-enzymatic transhydrogenation between NAD^+ and 1, 6-NADH.[48-49] Due to the lack of substrate coordination as in the mediator involved system, the obtained mediator-free NADH regeneration is poor in selectivity. For overcoming the poor selectivity problem, experiments with metal-free biological mediators for NADH regeneration are currently in progress.[50]

Based on the above NADH regeneration and its mechanism analysis, we performed the photoenzymatic synthesis of L-lactate assisting by L-lactate dehydrogenase (EC 1.1.1.27).[51] The synthesis of L-lactate from pyruvate will provide a way for oxidize NADH to NAD^+ for glycolysis when no oxygen is present. The enzymatic reaction is depicted in **Figure 6a**.

Firstly, the as-regenerated NADH is used to reduce pyruvate in the presence of L-lactate dehydrogenase. The NADH absorbance peak at 340 nm vanished within 5 minutes after addition of pyruvate solution and L-lactate dehydrogenase, which means that NADH is completely consumed for the L-lactate formation (**Figure S9a** of **ESI**). The two peaks around 300 nm are due to the characteristic absorbance of **M** in aqueous solution. **Figure S9b** of ESI shows the pyruvate reduction to lactate by commercial NADH assisting by L-lactate dehydrogenase, also reflecting the complete consumption of NADH in the enzymatic reaction (**Figure S10** of ESI). The quantitative conversion demonstrates that the photocatalytic generated NADH is indeed in the active form (1, 4-isomer), i.e. the artificial photosynthesis system produces a biologically accepted "currency".

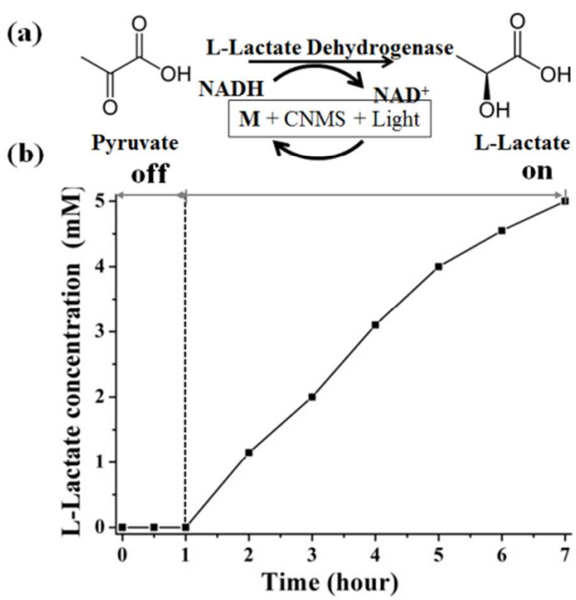

Figure 6. (a) The conversion between pyruvate and L-lactate by L-lactate dehydrogenase. (b) Photocatalytic propelled enzymatic synthesis of L-lactate by CNMS in the presence of **M** assisted by L-lactate dehydrogenase. Enzymatic reaction condition: NAD^+ (1 mM), M (0.25 mM), pyruvate (5 mM), L-Lactate dehydrogenase (50 U), pH=7.0 phosphate buffer with 15 w/v% TEOA, 3 mg CNMS.

The sustainable synthesis of L-lactate was achieved by coupling the mediator involved NADH photogeneration system with a redox enzyme, as illustrated in **Figure 6b**. The stoichiometry conversion of pyruvate to lactate was accomplished after 6 hours light illumination, using continuous reaction conditions. During the light reaction, the in-situ regenerated NADH was immediately consumed by L-lactate dehydrogenase for the synthesis of L-lactate from pyruvate, while the NAD^+ could be repeatedly regenerated (The molar ratio of pyruvate to NAD^+ was chosen to be 5, indicating the NADH must be continuously regenerated for accomplishing the stoichiometric conversion). The yield was determined by the integration of NMR signals of the starting and ending reaction solutions, as shown in **Figure S11** of ESI. During the dark cycle, there is no L-lactate product detected. Complete conversion of pyruvate to L-lactate could be verified by the NMR spectra. Therefore, we can safely state that it was possible to realize the photoenzymatic synthesis of L-lactate from pyruvate in the presence of L-lactate dehydrogenase. Through a coupling with other enzymes, we can imagine synthesizing more valuable compounds, but also small fuel molecules such as methanol.[52-56]

Conclusions

In conclusion, we presented a highly efficient cofactor regeneration systems which was synthesized by rational design and engineering of an existing photocatalytic system. Carbon nitride mesoporous spheres with bioinspired inner structure were synthesized for the first time and employed as the catalyst for photocatalytic NADH regeneration in the presence of a hydride transfer reagent. The high surface area and strong light harvesting capability ensures that the CNMS possesses the highest activity for NADH regeneration in the examined series. In a mediator free system, the CNMS also gives the best performance for NADH regeneration but with poor 1, 4 versus 1, 6-selectivity. The in-situ photocatalytic regenerated NADH could be coupled with L-lactate dehydrogenase for the synthesis of chiral L-lactate from pyruvate, and this reaction was run in a continuous fashion. This opens a general pathway for enzymatic synthesis of diverse chiral organic compounds, using ordinary light as the energy source. Owing to the facile synthesis and superior performance of CNMS, carbon nitride photocatalysis for NADH regeneration could turn compatible with the industrial demands for sustainable, high throughput synthesis. Furthermore, the silica-etching strategy for CNMS synthesis presented here could be extended to other nanomorphologies, the influence of which on reactivity stayed unexplored here, as well as to other compositions of heterogeneous photocatalysts. The synthesis sequence developed here thereby might open further possibilities to engineer high efficiency artificial photosynthesis systems in the future.

Notes and references

[a] Department of Colloid Chemistry, Max-Planck Institute of Colloids and Interfaces, Research Campus Golm, 14476 Potsdam (Germany)
E-mail: Jian.Liu@mpikg.mpg.de .
[b] College of Environmental and Biological Engineering, Putian University, Putian 351100, P.R.China.

Acknowledgement

J. L. acknowledges the support from Alexander von Humboldt Foundation. J. H. acknowledges the support from National Natural

Science Foundation of China (21103095) and the Excellent Young Scientific Research Talents in University of Fujian, China (JA12285). Dr. Guo Liang Li and Dr. Changqing Ye are acknowledged for helpful discussions and experimental assistance.

† Footnotes should appear here. These might include comments relevant to but not central to the matter under discussion, limited experimental and spectral data, and crystallographic data.
Electronic Supplementary Information (ESI) available: [Experimental section, TEM images, N_2 sorption isotherm plots, Time-resolved Photoluminescence, NMR spectra of CNMS can be found in ESI]. See DOI: 10.1039/c000000x/

1 J. Barber, *Chem. Soc. Rev.* **2008**, *38*, 185.
2 D. G. Nocera, *Acc. Chem. Res.* **2012**, *45*, 767.
3 H. Li, P. H. Opgenorth, D. G. Wernick, S. Rogers, T.-Y. Wu, W. Higashide, P. Malati, Y.-X. Huo, K. M. Cho, J. C. Liao, *Science* **2012**, *335*, 1596.
4 F. Wang, W. J. Liang, J. X. Jian, C. B. Li, B. Chen, C. H. Tung, L. Z. Wu, *Angew. Chem., Int. Ed.* **2013**, *52*, 8134.
5 S. Fukuzumi, Phys. Chem. Chem. Phys., **2008**, *10*, 2283–2297;
6 S. Fukuzumi, K. Doi, A. Itoh, T. Suenobu, K. Ohkubo, Y. Yamada, K. D. Karlin, *Proc. Natl. Acad. Sci. U. S. A.***2012**, *109,* 15572-15577.
7 M. L. Ghirardi, A. Dubini, J. Yu, P.-C. Maness, *Chem. Soc. Rev.* **2009**, *38*, 52.
8 S. J. Benkovic, S. Hammes-Schiffer, *Science* **2003**, *301*, 1196.
9 P. Könst, H. Merkens, S. Kara, S. Kochius, A. Vogel, R. Zuhse, D. Holtmann, I. W. Arends, F. Hollmann, *Angew. Chem., Int. Ed.* **2012**, *51*, 9914.
10 S. Staudt, E. Burda, C. Giese, C. A. Müller, J. Marienhagen, U. Schwaneberg, W. Hummel, K. Drauz, H. Gröger, *Angew. Chem., Int. Ed.* **2013**, *52*, 2359.
11 H. K. Chenault, G. M. Whitesides, *Appl. Bochem. Biotechnol.* **1987**, *14*, 147.
12 K. Seelbach, B. Riebel, W. Hummel, M. R. Kula, V. I. Tishkov, A. M. Egorov, C. Wandrey, U. Kragl, *Tetrahedron Lett.* **1996**, *37*, 1377.
13 A. Bardea, E. Katz, A. F. Bückmann, I. Willner, *J. Am. Chem. Soc.* **1997**, *119*, 9114.
14 H. C. Lo, R. H. Fish, *Angew. Chem., Int. Ed.* **2002**, *41*, 478.
15 R. Wichmann, D. Vasic-Racki, in *Technology transfer in biotechnology*, Springer, 2005, 225.
16 W. Ma, D.-W. Li, T. C. Sutherland, Y. Li, Y.-T. Long, H.-Y. Chen, *J. Am. Chem. Soc.* **2011**, *133*, 12366.
17 F. Hollmann, B. Witholt, A. Schmid, *J. Mol. Catal. B: Enzym.* **2002**, *19*, 167.
18 Z. Jiang, C. Lü, H. Wu, *Ind. Eng. Chem. Res.* **2005**, *44*, 4165.
19 J. Ryu, S. H. Lee, D. H. Nam, C. B. Park, *Adv. Mater.* **2011**, *23*, 1883.
20 Y. Maenaka, T. Suenobu, S. Fukuzumi, *J. Am. Chem. Soc.* **2012**, *134*, 367.
21 S. S. Bhoware, K. Y. Kim, J. A. Kim, Q. Wu, J. Kim, *J. Phys. Chem. C* **2011**, *115*, 2553.
22 S. Choudhury, J. O. Baeg, N. J. Park, R. K. Yadav, *Angew. Chem., Int. Ed.* **2012**, *124*, 11792.
23 J. H. Kim, M. Lee, J. S. Lee, C. B. Park, *Angew. Chem., Int. Ed.* **2012**, *51*, 517.
24 A. R. Parker, H. E. Townley, *Nat. Nanotechnol.* **2007**, *2*, 347.
25 X. Wang, K. Maeda, A. Thomas, K. Takanabe, G. Xin, J. M. Carlsson, K. Domen, M. Antonietti, *Nat. Mater.* **2008**, *8*, 76.
26 F. Goettmann, A. Fischer, M. Antonietti, A. Thomas, *Angew. Chem., Int. Ed.* **2006**, *45*, 4467.
27 Y. Wang, X. Wang, M. Antonietti, *Angew. Chem., Int. Ed.* **2012**, *51*, 68.
28 X. Zhang, X. Xie, H. Wang, J. Zhang, B. Pan, Y. Xie, *J. Am. Chem. Soc.* **2012**, *135*, 18.
29 G. Liu, P. Niu, C. Sun, S. C. Smith, Z. Chen, G. Q. Lu, H.-M. Cheng, *J. Am. Chem. Soc.* **2010**, *132*, 11642.
30 Y. S. Jun, J. Park, S. U. Lee, A. Thomas, W. H. Hong, G. D. Stucky, *Angew. Chem.* **2013**, *125*, 11289.
31 Y. Zhang, Z. Schnepp, J. Cao, S. Ouyang, Y. Li, J. Ye, S. Liu, *Sci. Rep.* **2013**, *3*, 2163.
32 S. Yang, Y. Gong, J. Zhang, L. Zhan, L. Ma, Z. Fang, R. Vajtai, X. Wang, P. M. Ajayan, *Adv. Mater.*, **2013**, 25, 2452.
33 J. Liu, M. Antonietti, *Energy Environ. Sci.* **2013**, *6*, 1486.
34 J. Toster, K. S. Iyer, W. Xiang, F. Rosei, L. Spiccia, C. L. Raston, *Nanoscale* **2013**, *5*, 873.
35 J. Liu, J. Huang, D. Dontsova, M. Antonietti, *RSC Adv.* **2013**, *3*, 22988.
36 Q. Yang, M. Li, J. Liu, W. Shen, C. Ye, X. Shi, L. Jiang, Y. Song, *J. Mater. Chem. A* **2013**, *1*, 541.
37 J. Liu, M. Li, J. Wang, Y. Song, L. Jiang, T. Murakami, A. Fujishima, *Environ. Sci. Technol.* **2009**, *43*, 9425.
38 J. Liu, G. Liu, M. Li, W. Shen, Z. Liu, J. Wang, J. Zhao, L. Jiang, Y. Song, *Energy Environ. Sci.* **2010**, *3*, 1503.
39 A. Zebda, C. Gondran, A. Le Goff, M. Holzinger, P. Cinquin, S. Cosnier, *Nat. Commun.* **2011**, *2*, 370.
40 Q. Zhang, T. Zhang, J. Ge, Y. Yin, *Nano Lett.* **2008**, *8*, 2867.
41 X. Wang, K. Maeda, X. Chen, K. Takanabe, K. Domen, Y. Hou, X. Fu, M. Antonietti, *J. Am. Chem. Soc.* **2009**, *131*, 1680.
42 Z. Dong, X. Lai, J. E. Halpert, N. Yang, L. Yi, J. Zhai, D. Wang, Z. Tang, L. Jiang, *Adv. Mater.* **2012**, *24*, 1046.
43 H. Li, Z. Bian, J. Zhu, D. Zhang, G. Li, Y. Huo, H. Li, Y. Lu, *J. Am. Chem. Soc.* **2007**, *129*, 8406.
44 I. G. Yu, Y. J. Kim, H. J. Kim, C. Lee, W. I. Lee, *J. Mater. Chem.* **2011**, *21*, 532.
45 H. Zhou, Z. Zhang, P. Yu, L. Su, T. Ohsaka, L. Mao, *Langmuir* **2010**, *26*, 6028.
46 M. V. Jose, S. Marx, H. Murata, R. R. Koepsel, A. J. Russell, *Carbon* **2012**, *50*, 4010.
47 J. Moiroux, P. J. Elving, *J. Electroanal. Chem. Interfacial Electrochem.* **1979**, *102*, 93.
48 P.J. Elving, W. T. Bresnahan, J. Moiroux, Z. Samec, Bioelectrochem. Bioenerg., 1982, 9, 365-378.
49 Y. Ohnishi, Y. Kikuchi, M. Kitami, *Tetrahedron Lett.*, **1979**, 32, 3005-3008.
50 Y.-T. Long, H.-Y. Chen, *J. Electroanal. Chem.* **1997**, *440*, 239.
51 R. K. Yadav, J.-O. Baeg, G. H. Oh, N.-J. Park, K.-J. Kong, J. Kim, D. W. Hwang, S. K. Biswas, *J. Am. Chem. Soc.* **2012**, *134*, 11455.
52 R. Obert, B. C. Dave, *J. Am. Chem. Soc.* **1999**, *121*, 12192.
53 R. Cazelles, J. Drone, F. Fajula, O. Ersen, S. Moldovan, A. Galarneau, *New J. Chem.* **2013**, *37*, 3721.
54 T. Reda, C. M. Plugge, N. J. Abram, J. Hirst, *Proc. Natl. Acad. Sci. U. S. A.* **2008**, *105*, 10654.
55 T. W. Woolerton, S. Sheard, E. Reisner, E. Pierce, S. W. Ragsdale, F. A. Armstrong, *J. Am. Chem. Soc.* **2010**, *132*, 2132.

56 Q. Sun, Y. Jiang, Z. Jiang, L. Zhang, X. Sun, J. Li, *Ind. Eng. Chem. Res.* **2009**, *48*, 4210.